Detecting People in Large Crowded Spaces Using 3D Data from Multiple Cameras*

João Carvalho[1], Manuel Marques[1], João Paulo Costeira[1] and Pedro Mendes Jorge[2]
[1]*Institute for Systems and Robotics (ISR/IST), LARSyS, Instituto Superior Técnico, Univ. Lisboa, Lisbon, Portugal*
[2]*ISEL - Instituto Politécnico de Lisboa, Lisbon, Portugal*
{jcarvalho, manuel, jpc}@isr.ist.utl.pt, pjorge@deetc.isel.pt

Keywords: 3D Point Cloud, Depth Camera, Multiple Cameras, Human Detection, Human Classification

Abstract: Real time monitoring of large infrastructures has human detection as a core task. Since the people anonymity is a hard constraint in these scenarios, video cameras can not be used. This paper presents a low cost solution for real time people detection in large crowded environments using multiple depth cameras. In order to detect people, binary classifiers (person/notperson) were proposed based on different sets of features. It is shown that good classification performance can be achieved choosing a small set of simple feature.

1 INTRODUCTION

Automatic human detection through 3D camera data is a core problem in many contexts. Examples are surveillance, human-robot interaction and human behaviour analysis. In this paper, it is proposed a methodology with depth cameras for people detection in large crowded spaces while maintaining the anonymity. The detection should be done in real time and without using color information, in order to preserve anonymity. These constraints are requested by the real world scenario: the monitoring of waiting queues and passages on an airport. Furthermore, the characteristics of the areas to cover imply the use of multiple depth cameras. The presented strategy segments candidates from the cameras data and classifies them into person or non-person. The procedure was tested on a labelled dataset with several subsets of features, in order to find one that requires low computational effort while still achieving good results.

1.1 Related Work

Extensive literature is available regarding human detection on RGB images (Moeslund et al., 2006). In (Mikolajczyk et al., 2004), the authors propose a method to detect people by using multiple body parts detectors. A widely used approach to detect humans in color images is to use the Histogram of Oriented Gradients (HOG) descriptor (Dalal and Triggs, 2005). To compute it, a given region of an image is divided into a number of cells and for each cell the gradient of its pixels is computed. The resulting gradients are then integrated into a histogram. To avoid the exhaustive process of sliding windows in search of candidates, several methods have been proposed to efficiently identify relevant regions of an image, such as (Zhu et al., 2006). Stereo camera systems have also allowed to achieve good results by estimating the depth of the covered areas (Ess et al., 2009).To add the three-dimensional information to video images, the integration with laser range finders has been frequently studied (Arras et al., 2007).
With the appearance of cheap depth cameras, such as the Asus Xtion[2], it became easy to merge color and 3D information in RGB-D images. Several methods have been proposed to perform human detection with such data. In (Spinello and Arras, 2011), the authors propose the Histogram of Oriented Depth (HOD) descriptor and combine it with the HOG descriptor, with an approach that implies each frame to be exhaustively scanned for people, implying a GPU implementation for real time usage. An alternative method is proposed in (Mitzel and Leibe, 2011), where the people detection is performed only in a set of regions of interest (ROI). However, the process of finding these

*Carvalho, Marques and Costeira were supported by the Portuguese Foundation for Science and Technology through the project LARSyS - ISR [UID/EEA/50009/2013]. Jorge was supported by SMART-er LISBOA-01-0202-FEDER-021620/SMART-er/QREN.

[2]`http://www.asus.com/3D-Sensor/Xtion_PRO/specifications/`

regions requires a GPU implementation. In (Munaro et al., 2012), it is proposed a fast solution to detect people within groups using the depth data. The candidates found are filtered by computing the HOG features of the RGB region corresponding to the candidates. A similar approach is proposed in (Liu et al., 2015), where the segmentation is also done using the 3D data followed by classification using a histogram of height difference and a joint histogram of color and height.
The methods referred all have the color information as an important part of the detection or classification procedure. However, there are cases where privacy and identity protection should be enforced. In such cases, RGB cameras must be avoided to prevent easy identification of the subjects involved. Work has been proposed that uses only the depth information. In (Xia et al., 2011), a two-stage head detection process is employed, with a first stage where a 2D edge detector finds a first set of candidates in the depth image, which are then selected using a 3D head model. The contour of the body is then extracted with a region growing algorithm. In (Bondi et al., 2014), the heads are detected by applying edge detection techniques to the depth images. The heads detection can be also achieved in a probabilistic approach (Lin et al., 2013). In (Hegger et al., 2013), the 3D data is divided in several layers according to its height and clustered using euclidean clustering. Each cluster is then classified using the histogram of local surface features and the clusters merged using connected components, with a final stage of classification of the merged clusters. In (Choi et al., 2013), the authors present a method to segment the depth image using a graph-based algorithm to determine ROIs. The HOD descriptor is then computed for each ROI and classified with a linear SVM. Other solution, (Brscic et al., 2013), uses low cost depth cameras and high resolution laser range finders for large scale infrastructures.

1.2 Outline

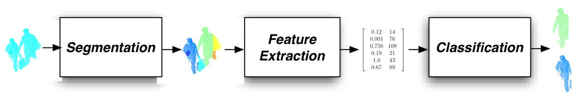

Figure 1: Methodology Outline. Three steps: segmentation, feature extraction; classification.

The outline of the proposed method is presented on Figure 1. The segmentation procedure is described in Section 3. Section 4 presents the set of features extracted from each candidate. Afterwards, on Section 5, the classification methods tested on this work are presented. Section 6 presents the labelled dataset created for this work. The results obtained are exposed on Section 7, followed by the future work and conclusions. Following, one presents the waiting queue scenario, camera setup and its challenges.

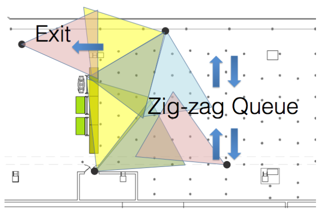

(a) Camera approximate setup

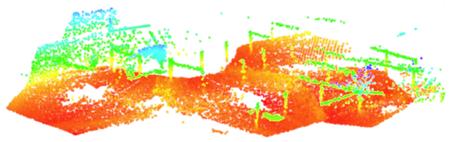

(b) A 3D point-cloud of the covered area

Figure 2: Waiting queue area camera setup: (a) approximate camera locations and field of view; (b) a 3D point-cloud of the covered area.

2 REAL SCENARIO CHALLENGES

To monitor the area of interest, one needs to compute several metrics, some of which require the full coverage of the space. Given the limited field of view (FOV) and range of depth cameras, this implies the use of multiple cameras. However, although one needs to completely cover the area, the overlap between cameras should be left to minimum, in order to avoid the degradation of the data by the interference of overlapping infrared patterns. Additionally, with limited and low height locations to place the cameras, several challenges are raised.
Figure 2a roughly illustrates the placement and FOV of the depth cameras used to cover our real world environment, a waiting queue area in a transportation infrastructure. Figure 2b presents a point cloud of the space captured without people. Note the visible zig-zag queue guides. The cameras required accurate calibration to ensure that the transition of people from one camera to another would be as "smooth" as possible. Very good intrinsic parameters are required to guarantee that the cameras report the depth information as close as possible to the true depth. Given a proper set of intrinsic parameters, cameras require extrinsic calibration to ensure that the relative pose of the cameras is as close as possible to the true value. How-

(a) Frontal view

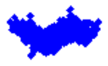
(b) Top view

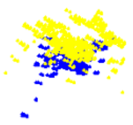
(c) Top view at 5.3m (data from two cameras)

Figure 3: Point-cloud of a person: (a) frontal view (of points with height above 1.30m) at about 3.3m from the camera; (b) top view on the same location as in (a); (c) top view on an area covered by two cameras, both at about 5.3m. The data points of each camera are presented in different colors.

ever, even with a good calibration, the point clouds from overlapping cameras will never match perfectly, leading to much noisier/fuzzier data. Additionally, the cameras used, Asus Xtion PRO, have a maximum specified depth range of 3.5m. In practice, however, to ensure full coverage, the depth data was used up to 5.5m. One should note that as distance increases, the camera loses precision and the data becomes noisier. Moreover, the ceiling of the area had a low height and the cameras were fixed at 2.3m from the ground. Having to cover a distance of 5.5m from the mounting point, this easily leads to severe occlusion of the people in the queue. Figure 3a presents the point cloud of the frontal view a person (only points with height above 1.30m) as viewed by a single camera at about 3.30m from the camera. Figure 3b presents the same person, at the exact same position but viewed from the top. Finally, Figure 3c presents the point-cloud of the same person from the top view on an area covered by two cameras. The point-cloud is now much more scattered and hardly (if) recognisable as a person profile. Therefore, this setup leads to point clouds of very occluded people or fuzzy point clouds.

3 DATA SEGMENTATION

This section presents the strategy used for the 3D point cloud segmentation. This procedure was originally inspired by the method described in (Munaro et al., 2012).

It should be noted that prior to the segmentation process, background subtraction is applied to the depth images and the 3D data is transformed to the global reference frame.

To illustrate the segmentation process, consider the depth image in Figure 4a and the point cloud of the closest foreground points, Figure 4b. Having the 3D points in a global reference plane, the algorithm iteratively searches for the highest point and fits a fixed sized box around that point. This encloses/clusters the surrounding points within the box. Afterwards, the clustered points are removed from the cloud and the procedure is iteratively repeated until no further points are left to cluster. Figures 5a to 5c present the first three steps of the process and Figure 5d presents the final segmentation results, with one color per cluster. The goal of iterating through points of maximum height is that those points will be good candidates to "top of the head point" and a rough centroid of a person. By using a fixed size box, one is assuming that a person occupies a maximum volume and that people keep a certain minimum distance from each other. In the presented example, despite successfully segmenting the two perceptible people (green and bigger blue clusters), another four clusters are extracted. Therefore, a classification strategy must be used to filter the candidates.

Finally, note that while iterating through points of maximum height, one only considers those points to be a valid head point if it has a minimum number of points bellow itself. This allows to further filter out spurious high points that might degrade the segmentation results.

Figure 6 presents a point cloud of the waiting queue with several people and the result of applying the segmentation procedure. Each cluster is displayed with a unique color, although very similar colors exist.

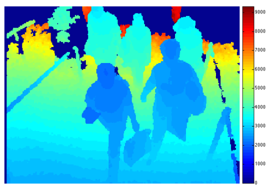
(a) Depth image

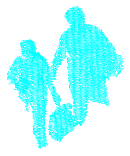
(b) Partial point cloud

Figure 4: Example of a depth image and partial point cloud: (a) presents a depth image form the camera on exit 1; (b) presents the point cloud of closest foreground points.

4 FEATURE EXTRACTION

In order to successfully classify candidate clusters, a set of relevant features must be extracted from the point clouds. Having the requirement to segment and classify dozens of point clouds in real-time, features should be computationally light. Computation of normal vectors of points, principal component analysis, (Hastie et al., 2009), or computationally demanding procedures as such, can not be used.

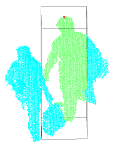
(a) Step 1

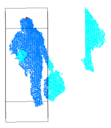
(b) Step 2

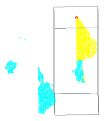
(c) Step 3

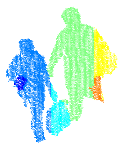
(d) Final

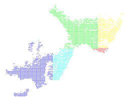
(e) Final - topview

Figure 5: Segmentation example: (a) to (c) frontal view of the first three steps of the segmentation process with box and highest point in red; (d) frontal view of the point cloud final segmentation; (e) top view of the point cloud final segmentation.

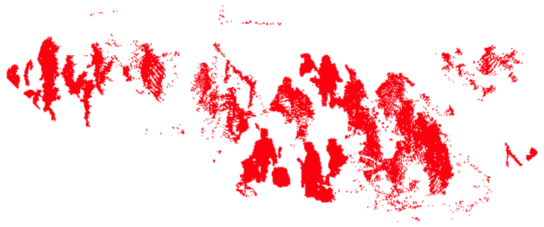
(a) Point cloud to segment

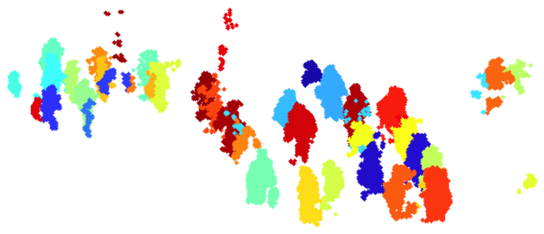
(b) Segmented point cloud

Figure 6: Example of the segmentation results for the waiting queue point cloud: (a) point cloud prior to segmentation; (b) segmented point cloud, one color per cluster (very similar colors exist).

The first features to extract from a candidate point cloud are the simplest features computed in this work: the *number of points* of each cluster; the *height* of the cloud, *i.e.*, the height of the highest point; and the *area* occupied by a cloud when its points are projected into the ground. Following, to account for the shape of the point cloud, a vector of features resulting directly from the segmentation is built. This is what one defines as *voxels*. For each segmented cluster, fit a fixed size box, centered exactly on its highest point. Afterwards, the box is divided by a regular grid, where each cell of that grid, a *voxel*, is set to one if at least one data point is in it and zero otherwise. For this work, the box has dimensions $0.66m * 0.66m * 2.1m$. Figure 7a presents an example of a voxelized point cloud with a voxel matrix of $11 * 11 * 35$, *i.e.*, with $0.06m$ size voxel. This grid of voxels is then vectorized and used as feature vector.

Other features to be used are the *ground projection of the heights* and the *ground projection of the number of points*. Both projections are represented by a $11 * 11$ matrix, dimensions equal to the first two dimensions of the voxel grid. The number of points (in fact, number of voxels) projection is the sum of the voxel cells along the third dimension of the grid (recall that voxel cells have $0/1$ value). Figure 7c presents such a matrix. On the heights projection, each cell of the matrix contains the height of the highest point falling into that cell, Figure 7b. Similarly, to the voxels, these matrix are vectorized to be used as feature vector.
Finally, a more complex descritor is computed, the *Ensemble of Shape Functions* (ESF), proposed in (Wohlkinger and Vincze, 2011). It considers distances between pairs of sampled points, angles between lines formed by three sampled points and areas of triangles built using randomly sampled points.
In summary, the full set of features is:

- number of points;
- height;
- area;
- heights projection;
- number of points projection;
- voxels;
- ESF.

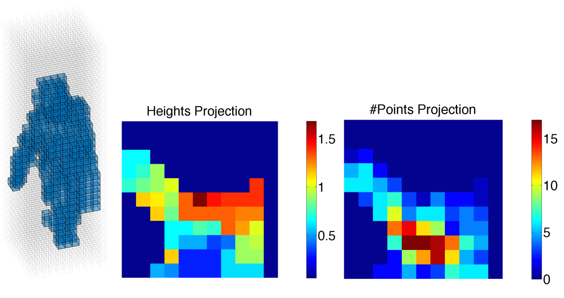

(a) (b) (c)

Figure 7: Feature examples: (a) voxels; (b) heights projection on the ground; (c) number of points projection on the ground.

5 CLASSIFICATION METHODS

This section presents the two classifiers tested for this human detection procedure, the *Support Vector Machine* (SVM), (Cortes and Vapnik, 1995), and the *Random Forest* (RF), (Breiman, 2001).

5.1 Support Vector Machine

A support vector classifier is a binary classification method that computes a hyperplane to separate observation points from two distinct classes. The goal is to find the hyperplane to which the distance between the observation points and the hyperplane is maximum. The computation of this hyperplane is done by solving the optimization problem

$$\begin{aligned} \max_{\beta_0,\beta,\varepsilon_1,\ldots,\varepsilon_N} \quad & M \\ \text{s.t.} \quad & y_i(\beta_0 + \beta^T x_i) \geq M(1-\varepsilon_i) \\ & ||\beta|| = 1 \\ & \varepsilon_i \geq 0 \\ & \sum_{i=1}^{N} \varepsilon_i \leq C, \end{aligned}$$

for all $i \in \{1,\ldots,N\}$. M is the separating margin, ε_i are the slack variables and C is a non-negative constant. By forcing the last constraint, one is imposing a bound on the margin and hyperplane violations. Therefore, if $C = 0$ no margin violation is allowed. When C is small, the margin is small and rarely violated. When C is large, the margin is wider and more violations are allowed. The C parameter is normally chosen through *cross-validation* (CV).
On this work, besides the linear classification on the original feature space, one also maps the features to a higher-dimensional space by using a SVM with a gaussian kernel:

$$K(x,\tilde{x}) = \exp\left(-\gamma||x-\tilde{x}||^2\right).$$

For further information on SVM, refer to (Cortes and Vapnik, 1995) and (Hastie et al., 2009).

5.2 Random Forests

Random forests is a method based on *decision trees*, (Breiman, 2001). Decision trees are capable of capturing complex structures in data and have relatively low bias. However, they are noisy, suffering from high variance. Random forests improve decision trees by reducing their variance and consequently decreasing their error rate. This is achieved by decreasing the correlation between trees, training each tree with different subset of the data points and by randomly selecting a subset of features at each node split.
RF allow the estimation the generalization error without using CV. The observations not used in the training of a tree are called *out-of-bag* (OOB) observations. For each point in the dataset, one can select the trees in which the point was OOB and get the classification of that point for each of those trees and get a final result through majority vote. The OOB classification error can be computed by applying this procedure to every point on the dataset. It can be shown that the OOB error is equivalent to the leave-one-out cross-validation error for sufficiently large number of trees.
Another interesting characteristic of the RF is the capability of assessing feature importance. After the RF training, to compute the importance of a particular feature, one randomly permutes the values of that feature across the OOB points and recomputes the error. The diference in the classification accuracy from the original OOB points and the permuted ones gives a measure of importance of the feature.
For further information on RF, refer to (Breiman, 2001) and (Hastie et al., 2009).

6 DATASET LABELLING

A dataset was built for this work by manually labelling segmented point clouds. To perform the labelling, the data was visually inspected. The raw data of the dataset, acquired at an airport, consists of images from eight depth cameras. Seven from the area presented on Figure 2 and an additional one from a close area. The 3D point clouds were computed from these images, segmented and merged on a global reference frame. Although the point clouds could have been labelled separately for each camera, the intent was to use the data as it was used on the referred project, with overlapping areas.

Although in this work only two classes are considered for classification, person or non-person, the point clouds were labelled in four classes: complete person, waist up person, shoulders up person and non-person. The reason is that there exists frequent occlusion when the space is crowded, and by labelling people depending on their visibility one can more easily inspect classification results and hopefully understand better in which cases the classifier fails. Figure 8 presents and observation from each of the person classes. Please note that for training the classifiers, these three classes were merge into a unique one. Note also that the dataset is noisy. People can be observed from several views, from the front, from

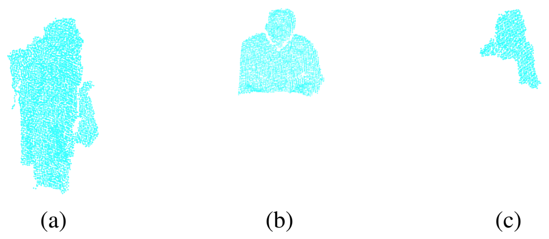

Figure 8: Example of an observation per person class: (a) complete person observation, sideways, with backpack; (b) waist up person observation, frontal view; (c) shoulders up person observation, slightly sideways.

the back, sideways or something in-between. Also, as previously referred, the point clouds get noisier with the distance from the cameras as on the areas where the data from multiple cameras overlap.
A total of 1345 point clouds were labelled, with 542 non-people, 545 complete body people, 183 waist up people and 75 shoulders up people.

7 EXPERIMENTAL RESULTS

As referred in the previous section, the three person classes were merged into a unique one. To balance the dataset, the observations corresponding to complete body people were down sampled such that the total number of person observations matches the number of non-people.
From this dataset, the features described in Section 4 were computed and applied standardization to all of them. Also, features with null standard deviation (features equal for all points on the dataset) were removed. With these features, several subsets were built to train the classifiers:

- *f1*: $\{\text{heights, number of points, areas}\} \in \mathbb{R}^3$;
- *f2*: $\{\text{heights projection}\} \in \mathbb{R}^{121}$;
- *f3*: $\{\text{number of points projection}\} \in \mathbb{R}^{121}$;
- *f4*: $\{f1, f2, f3\} \in \mathbb{R}^{245}$;
- *f5*: $\{\text{voxels}\} \in \mathbb{R}^{3390}$;
- *f6*: $\{\text{ESF}\} \in \mathbb{R}^{612}$;
- *f7*: $\{f4, f5, f6\} \in \mathbb{R}^{4247}$.

The purpose of this feature separation into several subsets is to assess their performance versus all the features, *f7*. For each subset, training was done for a SVM with linear kernel, a SVM with gaussian kernel and a random forest.
For training and validation purposes, the dataset was divided into training and test data, with 759 observations ($\sim 70\%$) and 325 observations, respectively.

Table 1: Training CV error rates for the linear SVM (LSVM), gaussian SVM (GSVM) and OOB error rate for the RF. The subset of features to which the classifier had lower error is in bold type.

	CV Error		OOB Error
	LSVM	*GSVM*	*RF*
f1	0.0501	0.0408	0.0461
f2	0.0514	0.0435	0.0422
f3	0.0988	0.0738	0.0646
f4	0.0277	0.0303	**0.0343**
f5	0.0382	**0.0290**	**0.0343**
f6	0.0856	0.0896	0.0725
f7	**0.0264**	**0.0290**	0.0369

Table 2: Classification error rates for the training and test datasets. The subset of features to which the classifier had lower error is in bold type. The lowest error for the test dataset is underlined.

	Test Data Error		
	LSVM	*GSVM*	*RF*
f1	0.0554	0.0554	0.0400
f2	0.1077	0.0923	0.0585
f3	0.1015	0.0677	0.0554
f4	0.0462	0.0523	0.0338
f5	**0.0400**	0.0400	0.0400
f6	0.0831	0.0862	0.0492
f7	0.0431	**0.0277**	**0.0246**

The SVMs were trained with 5-fold cross-validation in order to compute the best parameters for the classifier. For the linear kernel, one tested a total of 20 logarithmically spaced values of $C \in [10^{-5}, 10^5]$. For the gaussian kernel, one tested 10 values for $C \in [10^{-2}, 10^7]$ and 10 values for $\gamma \in [10^{-6}, 10^1]$. The parameters with lowest cross-validation error were chosen as the best ones and used to evaluate the model on the test dataset. The random forest was trained with 250 decision trees and $\sqrt{p}$ features chosen at each node split.
For testing the SVM classifiers, one used the MATLAB toolkit PMTK3[3]. For building the RFs, it was used the Statistics and Machine Learning Toolbox for MATLAB. All the features were implemented in MATLAB, with the exception for the ESF. The ESF is implemented in the PCL library (Rusu and Cousins, 2011).

Table 1 reports, for all feature sets, the CV error of each SVM "winning" model and the OOB error for the RF with 250 trees. The linear SVM (LSVM) achieves the lowest CV error, 0.0264, when using all the features, *f7*, but obtains a very close error for *f4*. For the gaussian SVM (GSVM), the best training re-

[3]https://github.com/probml/pmtk3 - PMTK3 webpage. Last accessed on August 26, 2015.

sults are obtained for *f5* and *f7*, with 0.0290 of error. For the random forests (RF), the lowest OOB error is obtained for *f4* and *f5*, with 0.0343, but with close results for *f7*.

Table 2 presents the classification error rate of each classifier and set of features for the test observations. The three classifiers had the exact same error rate for *f4*, however, for all the other subsets the RF outperformed the SVM classifiers. The best result was obtained using *f7*, with a 0.0246 error rate. The LSVM performed best for *f4*, with 0.0400 error rate, and the GSVM for *f7*, close to the RF result, with 0.0277.

Besides the lower error for the test dataset, the RF classifier has the advantage of being simple to train and not prone to overfitting (James et al., 2013). With RFs, assuming $m = \sqrt{p}$ as proposed by the authors, one only has to choose the number of trees to train. On the other hand, with the SVM, one has to choose a kernel, choose a range of values for the classifier and kernel parameters and use cross-validation to find the best values. Depending on the kernel used and number of parameter values tested, this can lead to long training times. For instance, with *f7*, the training of the RF took $14.13s$ of cpu time, while the SVMs took $83.18s$ and $1743.22s$ for the linear and gaussian kernels, respectively.

While training the RF for the *f7* feature set, the OOB feature importance was recorded. The three simplest features, *i.e.*, heights, number of points and areas, are exactly the features with higher importance, with 1, 0.9115 and 0.9119, respectively[4]. One should note that this tool evaluates the importance of each feature space dimension individually and that only these first three dimensions can be seen as individual. All the other dimensions of the space are part of "composed" features, such as the voxels or the ESF. So, even if the most important features are the three referred, the composed features end up having more importance when all of its dimensions are summed. Figure 9b presents the sum of feature importance by composed feature. One can see that the composed feature that has higher "summed" oob importance is the ESF. This comes a litle surprising as the ESF (*f6*) is far from being the best feature subset according to Table 2. From this one can conclude that even if the sum of the importante of a composed feature is much higher than some other feature, that does not necessarily mean that the composed feature will lead to lower error rates. Figure 9a presents the mean of the OOB feature importance for each composed feature. One can easilly understand that if one is to use a small number of features, the heights, the number of points and the area are the ones to use. The voxels have the

[4]Values normalized by the maximum importance value.

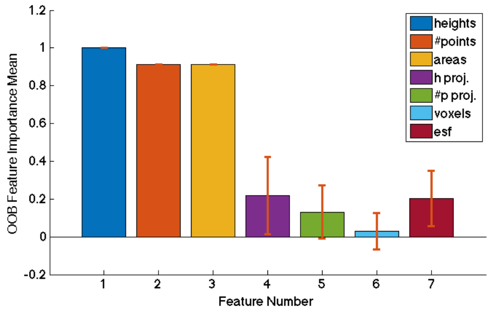

(a)

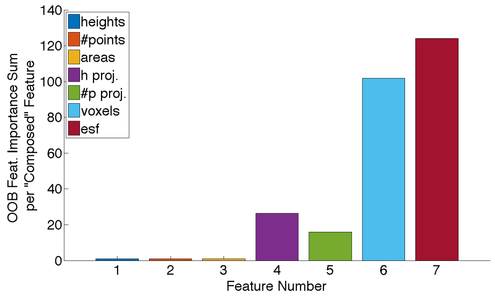

(b)

Figure 9: OBB Feature importance: (a) mean per "composed" feature set; (b) summed per "composed" feature set.

lowest mean, as many of its cells have negative importance, meaning they lead to the decrease of the accuracy. There are also zero importance cells, cells that made no difference in the classification or were never tested for node splitting.

The testing data set was formed by 159 non-person observations, 91 complete body observations, 53 waist up observations and 22 shoulders up observations. For each of these subclasses, the best LSVM misclassified 4.40%, 4.40%, 3.77% and 0%, respectively. The GSVM misclassified 3.77%, 1.10%, 3.77% and 0%. The RF misclassified 2.52%, 3.30%, 1.89% and 0%. These results show that, contrary to what could be expected, the classifiers do not present significant differences in misclassification percentage between the point clouds corresponding to occluded and non-occluded people. Further, the observations from people visible only from the shoulders up were all correctly classified.

To achieve real time performance, the segmentation and feature extraction procedures were implemented in C. The candidates are classified by a Python RF implementation (Pedregosa et al., 2011). The segmentation and classification procedures take around $0.2ms$ per person, for the *f1*. It must be noted that the segmentation implementation is not optimized and further improvements can be achieved.

8 CONCLUSIONS

This paper presented a low-cost solution for human detection in large infrastructures while preserving people identity. Real time performance is achieved by using a small set of simple features. It was presented a real scenario in which multiple depth cameras are simultaneously used to monitor the environment. The method uses the merged data from the cameras and finds candidates by segmenting the resulting 3D point cloud. For each candidate, a set of features is extracted. Several subsets of features were tested to assess their performance when used as input to a classifier. The proposed classifier lies on features with low computational cost and achieves good performance in a real time scenario.
As future work, it would be interesting to explore the creation of confidence regions on the FOV of each camera to account for the accuracy degradation with the distance.

ACKNOWLEDGEMENTS

The authors would like to thank João Mira, Thales Portugal S.A. and ANA *Aeroportos de Portugal* for enabling the data acquisition within the SMART-er project and Susana Brandão by providing the ESF MATLAB wrapper.

REFERENCES

Arras, K. O., Mozos, Ó. M., and Burgard, W. (2007). Using boosted features for the detection of people in 2d range data. In *IEEE ICRA*, pages 3402–3407. IEEE.

Bondi, E., Seidenari, L., Bagdanov, A. D., and Del Bimbo, A. (2014). Real-time people counting from depth imagery of crowded environments. In *Advanced Video and Signal Based Surveillance (AVSS), 11th IEEE International Conference on*, pages 337–342. IEEE.

Breiman, L. (2001). Random forests. *Machine learning*, 45(1):5–32.

Brscic, D., Kanda, T., Ikeda, T., and Miyashita, T. (2013). Person tracking in large public spaces using 3-d range sensors. *Human-Machine Systems, IEEE Transactions on*, 43(6):522–534.

Choi, B., Meriçli, C., Biswas, J., and Veloso, M. (2013). Fast human detection for indoor mobile robots using depth images. In *IEEE ICRA*, pages 1108–1113. IEEE.

Cortes, C. and Vapnik, V. (1995). Support-vector networks. *Machine learning*, 20(3):273–297.

Dalal, N. and Triggs, B. (2005). Histograms of oriented gradients for human detection. In *IEEE CVPR Computer Society Conference on*, volume 1, pages 886–893. IEEE.

Ess, A., Leibe, B., Schindler, K., and Van Gool, L. (2009). Moving obstacle detection in highly dynamic scenes. In *IEEE ICRA*, pages 56–63. IEEE.

Hastie, T., Tibshirani, R., and Friedman, J. (2009). The elements of statistical learning.

Hegger, F., Hochgeschwender, N., Kraetzschmar, G. K., and Ploeger, P. G. (2013). People detection in 3d point clouds using local surface normals. In *RoboCup 2012: Robot Soccer World Cup XVI*, pages 154–165. Springer.

James, G., Witten, D., Hastie, T., and Tibshirani, R. (2013). *An introduction to statistical learning*. Springer.

Lin, W.-C., Sun, S.-W., and Cheng, W.-H. (2013). Demo paper: A depth-based crowded heads detection system through a freely-located camera. In *IEEE ICME Workshops*, pages 1–2. IEEE.

Liu, J., Liu, Y., Zhang, G., Zhu, P., and Chen, Y. Q. (2015). Detecting and tracking people in real time with rgb-d camera. *Pattern Recognition Letters*, 53:16–23.

Mikolajczyk, K., Schmid, C., and Zisserman, A. (2004). Human detection based on a probabilistic assembly of robust part detectors. In *Computer Vision-ECCV*, pages 69–82. Springer.

Mitzel, D. and Leibe, B. (2011). Real-time multi-person tracking with detector assisted structure propagation. In *IEEE ICCV Workshops*, pages 974–981. IEEE.

Moeslund, T. B., Hilton, A., and Krüger, V. (2006). A survey of advances in vision-based human motion capture and analysis. *Computer vision and image understanding*, 104(2):90–126.

Munaro, M., Basso, F., and Menegatti, E. (2012). Tracking people within groups with rgb-d data. In *IEEE/RSJ IROS International Conference on*, pages 2101–2107. IEEE.

Pedregosa, F., Varoquaux, G., Gramfort, A., Michel, V., Thirion, B., Grisel, O., Blondel, M., Prettenhofer, P., Weiss, R., Dubourg, V., Vanderplas, J., Passos, A., Cournapeau, D., Brucher, M., Perrot, M., and Duchesnay, E. (2011). Scikit-learn: Machine learning in Python. *Journal of Machine Learning Research*, 12:2825–2830.

Rusu, R. B. and Cousins, S. (2011). 3D is here: Point Cloud Library (PCL). In *IEEE ICRA*, Shanghai, China.

Spinello, L. and Arras, K. O. (2011). People detection in rgb-d data. In *IEEE/RSJ IROS International Conference on*, pages 3838–3843. IEEE.

Wohlkinger, W. and Vincze, M. (2011). Ensemble of shape functions for 3d object classification. In *IEEE ROBIO International Conference on*, pages 2987–2992. IEEE.

Xia, L., Chen, C.-C., and Aggarwal, J. K. (2011). Human detection using depth information by kinect. In *IEEE CVPR Workshops Computer Society Conference on*, pages 15–22. IEEE.

Zhu, Q., Yeh, M.-C., Cheng, K.-T., and Avidan, S. (2006). Fast human detection using a cascade of histograms of oriented gradients. In *IEEE CVPR Computer Society Conference on*, volume 2, pages 1491–1498. IEEE.